

Fast Convex Relaxations using Graph Discretizations

Jonas Geiping¹, Fjedor Gaede², Hartmut Bauermeister¹ and Michael Moeller¹

¹Department of Electrical Engineering and Computer Science, University of Siegen
Hölderlinstraße 3, 57076 Siegen

{jonas.geiping, hartmut.bauermeister, michael.moeller}@uni-siegen.de

²Institut für Analysis und Numerik, Westfälische Wilhelms-Universität Münster
Orléans-Ring 10, 48149 Münster

fjedor.gaede@uni-muenster.de

March 10, 2021

Abstract

Matching and partitioning problems are fundamentals of computer vision applications with examples in multilabel segmentation, stereo estimation and optical-flow computation. These tasks can be posed as non-convex energy minimization problems and solved near-globally optimal by recent convex lifting approaches. Yet, applying these techniques comes with a significant computational effort, reducing their feasibility in practical applications. We discuss spatial discretization of continuous partitioning problems into a graph structure, generalizing discretization onto a Cartesian grid. This setup allows us to faithfully work on super-pixel graphs constructed by SLIC or Cut-Pursuit, massively decreasing the computational effort for lifted partitioning problems compared to a Cartesian grid, while optimal energy values remain similar: The global matching is still solved near-globally optimally. We discuss this methodology in detail and show examples in multi-label segmentation by minimal partitions and stereo estimation, where we demonstrate that the proposed graph discretization technique can reduce the runtime as well as the memory consumption by up to a factor of 10 in comparison to classical pixelwise discretizations.

1 Introduction

Matching problems and the closely inter-related minimal partitioning problems are low-level computer vision tasks that build a backbone for a variety of applications such as multi-label segmentation [3], stereo estimation [23, 45] and optical flow estimation [21, 7]. However, posing these problems as energy minimization problems leads to non-convex objectives that are difficult to solve. In the last years, it was demonstrated that functional lifting techniques are very well suited for solving these non-convex minimization problems via convex relaxations in a higher-dimensional space. Unfortunately, despite the precise solutions these methods provide, they incur significant costs in memory and computational effort, due to the high dimensionality of the lifted problem.

To be more technically precise, consider the continuous minimal partitions problem, also referred to as piecewise-constant Mumford-Shah problem [34], which builds the basis of the aforementioned computer vision applications,

$$\min_{\{P_k\}_{k=1}^L} \sum_{k=1}^L \int_{P_k} -f_k(x) + \frac{1}{2} \text{Per}(\Omega, P_k). \quad (1)$$



Figure 1: Graph discretization on the left and segmentation by convex relaxation, here piecewise-constant Mumford-Shah with 32 labels, computed on the graph structure on the right. This segmentation solution is 3.03% less optimal compared to the relaxation on a Cartesian grid sized as the original image data, but requires only around 4.8% of computation time, as the original problem has 4.9 million variables, and the reduced problem only 120k.

Given a set of L potential functions f_k we are looking for a partitioning of the set Ω into L non-overlapping partitions $\{P_k\}_{k=1}^L$, i.e. $P_k \cap P_l = \emptyset$ if $k \neq l$ and $\bigcup_{k=1}^L P_k = \Omega$ [9]. Without the regularizing perimeter term, the solution is given by $\arg \max_k f_k(x)$ for every $x \in \Omega$, but under inclusion of the second term in (1), the perimeter of each partition is penalized, leading to spatially coherent solutions, where every point is "matched" to a partition, but the global surface energy stays minimal.

Minimal partitions problems are abundant in imaging. In the discrete setting they directly relate to the Potts model [44] and MRF approaches [4, 3]. This variability hinges on the choice of potential functions f_k . For multi-label segmentation, for example, we can consider each f_k to give the prior likelihood that the point x should be assigned label k , with the likelihood being computed by model-based approaches [14] or returned as the output of a neural network [13]. On the other hand, considering every partition with label k to encode a displacement of k pixels between two stereo images, the same framework can be used to solve stereo matching problems [38, 59]. Further immediate examples include optical flow [21, 50], scene flow and multiview reconstruction [25].

To be able to solve Eq. (1), we need to minimize over a set of partitions. This discrete matching problem at the heart of the minimal partitions problem is in general NP-hard. The only cases in which it can be solved globally is if $L = 2$ [11] (paralleling binary cuts in the discrete setting) or if the partitioning is itself a continuous range, see [42]. In practice, one of the most powerful approaches is the solution of a suitable convex relaxation of the original minimal partitions problem. To do so, the minimization over partitions is first replaced by minimization over their characteristic functions $u_k : \Omega \rightarrow \{0, 1\}$, satisfying $\sum_{k=1}^L u_k(x) = 1 \quad \forall x \in \Omega$,

$$\min_{\{u_k\}_{k=1}^L} \sum_{k=1}^L \int_{\Omega} -f_k(x)u_k(x) + \int_{\Omega} |Du_k|, \quad (2)$$

where we have equivalently replaced the perimeter of a set by the total variation of its characteristic function, see [9]. In a next step, the functions u_k are relaxed to take values in the full interval $[0, 1]$, either directly [61, 31], or by jointly deriving tighter convex reformulations of the regularizer [9]. Relaxation approaches often leads to near-optimal solutions with high fidelity [43, 52], yet the computational effort amounts to solving a non-smooth, non-strongly convex optimization problem over all functions u_k , each of which is usually discretized to be as large as the given potential functions. Especially when k is large, memory costs quickly become impractical for computer vision applications.

In this work we hence consider strategies to remediate the computational costs of functional lifting techniques, without impeding their global matching capabilities. As illustrated in figure 1, we propose to first discretize the problem on a precomputed graph structure instead of a Cartesian grid, and then solve the convex relaxation on the graph. This strategy leads to significant computational advantages while sacrificing almost no accuracy in terms of the energy of the final solution.

2 Related Work

The minimal partitions problem is a prime example of energy minimization methods in computer vision [34, 47, 8], which have found widespread use. In the context of convex relaxations of these partition problems, there have been works in as diverse applications such as stereo estimation [43, 42, 55, 45, 46], optical flow [52, 19, 50], segmentation [37, 60, 61, 31, 40, 9], image processing [41], optimization on manifolds [32] and other applications [25, 5, 56], with algorithmic improvements such as [49]. See [14] for an overview.

An especially interesting algorithmic improvement are sublabel-accurate liftings introduced in [36, 30, 35]. For tasks such as stereo estimation and optical flow, where labels can be ordered, the number of labels can be significantly reduced by discretizing the continuous partitions appropriately. This technique greatly reduces the computational effort of functional lifting methods in a variety of applications. These improvements, however, discuss the discretization of the label space and are therefore an orthogonal direction of research to our work, as we are discussing compact discretizations of the image space.

Research on continuous relaxation approaches has much in common with its discrete counterparts in works such as [24, 23, 3], yet their differing viewpoints lead to interesting distinctions in applicability [4, 26], exactness of relaxation [22] and parallelizability [58].

Turning away from convex relaxation approaches, the choice of efficient discretization of the input image data can be clearly related to superpixels approaches, e.g. [1, 54]. Their general idea is to generically reduce the computational complexity of any (pixel-based) numerical algorithm, by locally grouping pixels of similar color to larger superpixels. The most prominent algorithm in current practice is SLIC (Simple Iterative Linear Clustering) [1]. However, for interface energies such as the minimal partitioning problems discussed here, the adherence to borders with minimal surface energy is crucial, as we will discuss later. Ideally, the superpixel setup should also be chosen by an appropriate minimization procedure that adheres to the perimeter construction. However, such approaches are generally too costly to be applied as a mere discretization step. Yet, an interesting exception is the Cut-Pursuit algorithm [27, 28], which solves total variation minimization and related problems in a fast sequence of binary graph cuts, making it competitive as a discretization step and leading to boundaries that better adhere with minimal partitions. This approach has been successfully applied in practice in such works as [29, 20] and we will contrapose a superpixel structure generated by Cut Pursuit with one generated by SLIC in our main comparison to a Cartesian grid.

3 Graph Discretizations for Convex Relaxations

3.1 Preliminaries

Let us first introduce our general notation. For the discrete setup we consider an undirected graph structure is defined by its vertices V , edges among vertices $E \subset V \times V$ and weights of these edges $w \in \mathbb{R}^{|E|}$. We refer to [16] for details.

The continuous minimal partition problem requires the definition of the total variation of a function $u \in L^1(\Omega, \mathbb{R}^L)$ as

$$TV(u) = \sup \left\{ - \int_{\Omega} \sum_{k=1}^L u_k(x) \operatorname{div} \mathbf{p}_k(x) dx, \right. \\ \left. \mathbf{p} \in C_c^1(\Omega, \mathbb{R}^{d \times L}), \sum_{k=1}^L |\mathbf{p}_k(x)|^2 \leq 1 \right\},$$

Note that the above definition reduces to $TV(u) = \sum_{k=1}^L \int_{\Omega} |\nabla u_k(x)| dx$ for smooth u . We define u to be an element of the space of bounded variation $BV(\Omega, \mathbb{R}^L)$ if $TV(u)$ is finite. We can then identify this value with the mass of the distributional derivative Du , i.e. $\int_{\Omega} |Du| = TV(u)$. According to [17], the bounded Radon measure Du can be decomposed into

$$Du = \nabla u \mathcal{L}^d + Cu + (u^+ - u^-) \otimes \nu_u \mathcal{H}^{d-1} \llcorner J_u, \quad (3)$$

where \mathcal{L}^d is the Lebesgue measure, J_u is the jump set of u , where $u^+ \neq u^-$, i.e. the values at the boundary differ, ν_u the normal of the boundary and Cu a remainder Cantor part. In the following we will consider functions $u \in SBV(\Omega, \mathbb{R}^L)$, where $Cu = 0$ [2, 35]. We further define the perimeter of a measurable set $P \subset \Omega$ in turn by the total variation of its characteristic function $\chi_P : \Omega \rightarrow \mathbb{R}$ [9], the boundary of a set as $\partial S = \bar{S} \setminus \operatorname{int}(S)$, and the length of the boundary $\Gamma_{k,l} = \partial P_k \cap \partial P_l$ between two sets P_k, P_l via

$$|\Gamma_{k,l}| = \mathcal{H}^{d-1}(\Gamma_{k,l}), \quad (4)$$

where, again, \mathcal{H}^{d-1} denotes the $d - 1$ -dimensional Hausdorff measure. These definitions basically allow us to examine the continuous boundary of shapes. Refer to Fig. 2a, where these continuous objects are marked in red.

3.2 Graph Discretization

We are interested in solving the continuous minimal partition problems Eq. (2) numerically. To do so we need to translate the problem into the discrete setting. To take a step from the continuous definitions to a discrete problem, we make use of the fact that we expect solutions u^* to the minimal partitioning problem to be piecewise constant with a finite number of pieces. In essence we want to choose a discretization to a finite setting that mimics these properties optimally: *We represent the structure of the discretization by a graph of candidate constant sets, the nodes of which represent each separate piece and where neighboring pieces are connected by edges in the graph.* After solving the resulting problem on the graph, the final solution u^* can be reassembled by labeling the constant regions according to the respective label of the node that represents it. This setup is sketched in Fig. 2.

Note that this is a generalization of a classical discretization to a Cartesian grid. Placing a continuous function on an pixel grid corresponds to claiming that the function is piecewise-constant on every image pixel - hence the boundaries of the solution u^* to the minimal partitions problem will be a subset of the boundaries imposed by the image pixels.

In slight generalization of the minimal partitions problem in Eq. (2) we now discuss the type of continuous functionals $F : BV(\Omega, \mathbb{R}^L) \rightarrow \mathbb{R}$, that we want to represent discretely. Due to the discontinuities of BV , we define different components of F on the continuous parts and the jump parts J_u of Eq. (3):

$$F(u) = \int_{\Omega \setminus J_u} \Phi(x, u(x), \nabla u(x)) dx \\ + \int_{J_u} \kappa(|u^+ - u^-|) |\nu_u| d\mathcal{H}^{d-1}, \quad (5)$$

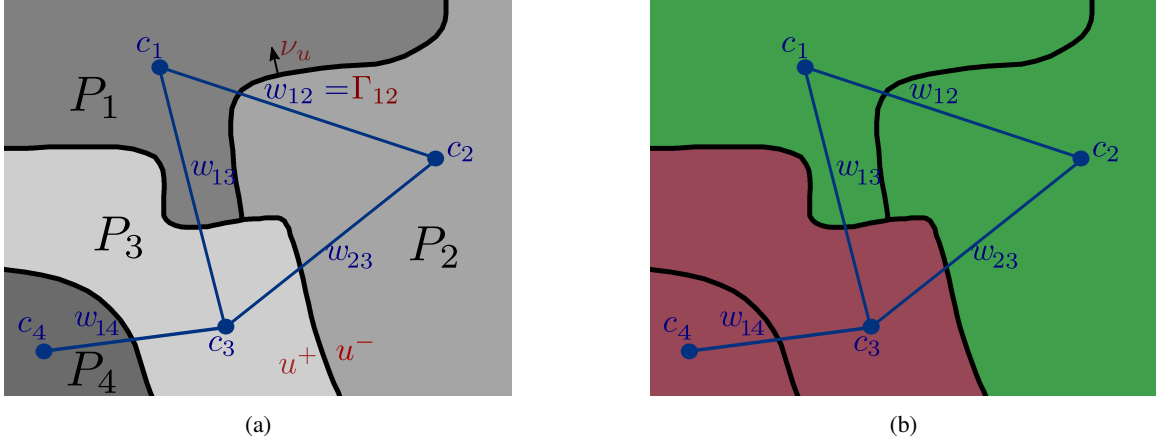


Figure 2: Sketch of the discretization process for a graph-based discretization. a) The underlying continuous function $u \in BV_{\Pi}(\Omega, \mathbb{R}^L)$ is pictured in black, with piecewise-constant partitions $\Pi = \{P_1, P_2, P_3, P_4\}$ shown in gray as well as the discrete graph structure in blue. b) A minimal partitions problem with two potentials is solved on this graph structure. Pictured is the solution u^* which now corresponds to a piecewise constant solution (in red and green) on the graph.

where ∇, u^+, u^- refer to the decomposition detailed in Eq. (3). $\Phi : \Omega \times \mathbb{R}^L \times \mathbb{R}^{L \times d} \rightarrow \mathbb{R}$ is a function defined away from the jump set of u , while $\kappa : \mathbb{R} \rightarrow \mathbb{R}$ is a concave function measuring the jump penalty with $\kappa(0) = 0$ [9, 35]. We can consider the first term to be a generalized data term, and the second as a (jump)-regularizer.

To connect the continuous formulation of Eq. (5) to a discrete setting we define the discretization as a finite set of candidate sets $\Pi = \{P_i \subset \Omega \mid P_i \cap P_j = \emptyset, \forall j \neq i\}$ with $M = |\Pi|$ partitions. The continuous function $u \in BV(\Omega, \mathbb{R}^L)$ is assumed to be constant on every partition, so that we can denote its value on partition $P_i \in \Pi$ by a vector $c_i \in \mathbb{R}^L$. Thus, $u(x) = c_i$ for every $x \in P_i \subset \Omega$. The partition Π can be represented by a set of nodes $V = \{1, \dots, M\}$ where each node corresponds to a segment $P_i \in \Pi$. Furthermore we can describe every boundary between sets P_i and P_j as Γ_{ij} and by that define an edge set $E \subset V \times V$ as $E = \{(i, j) \in V \times V \mid |\Gamma_{ij}| > 0, i \neq j\}$. Note, that the perimeter of some partition $P_i \in \Pi$ is given by $\text{Per}_{P_i} = \sum_{(i,j) \in E} |\Gamma_{ij}|$.

Let us assume that our desired solution u^* , which minimizes Eq. (5), is piecewise constant. More formally, given some partition Π let us write $u \in BV_{\Pi}(\Omega, \mathbb{R}^L)$ to denote continuous functions in BV which are piecewise constant on the regions in Π , and assume $u^* \in BV_{\Pi}(\Omega, \mathbb{R}^L)$. This implies that the jump set J_u is a subset of $\cup_{(i,j) \in E} \Gamma_{ij}$ and that $\Omega \setminus J_u$ is a subset $\cup_{i \in V} P_i$, or, in other words, the discretization by Π is able to represent the structure of u^* .

Under the above assumption we can restrict the minimization of F over all functions $u \in BV(\Omega, \mathbb{R}^L)$ to those in $BV_{\Pi}(\Omega, \mathbb{R}^L)$ which allows to simplify Eq. (5) to a problem in which merely the values c_i inside the piecewise constant regions are the unknowns. Let us discuss the three main components of Eq. (5) separately.

Data Term:

Considering F for any $u \in BV_\Pi(\Omega, \mathbb{R}^L)$ allows us to rewrite the first term of Eq. (5) as

$$\begin{aligned} K(u) &= \int_{\Omega \setminus J_u} \Phi(x, u(x), \nabla u(x)) \, dx \\ &= \sum_{i=1}^M \int_{P_i} \Phi(x, c_i, 0) \, dx \\ &=: K_\Pi(c) \end{aligned} \tag{6}$$

which is the discrete representation $K_\Pi(c) : \mathbb{R}^{M \times L} \rightarrow \mathbb{R}$ of this term that mere depends on the values c_i . For linear data terms such as in Eq. (2), i.e. $\Phi(x, u(x), \nabla u(x)) = \sum_{k=1}^L f_k(x) u_k(x) = f_k(x) (c_k)_i$ for $x \in P_i$, this is further simplified to

$$K_\Pi(c) = \sum_{k=1}^L \sum_{i=1}^M (c_i)_k \int_{P_i} f_k(x) \, dx = \sum_{i=1}^M \langle c_i, \tilde{f}_k \rangle \tag{7}$$

with $\tilde{f}_k = \left(\int_{P_i} f_k(x) dx \right)_{k=1}^L \in \mathbb{R}^L$.

Regularization Term:

For the jump regularization, we can write $R(u)$ for any $u \in BV_\Pi(\Omega, \mathbb{R}^L)$ as

$$\begin{aligned} R(u) &= \int_{J_u} \kappa(|u^+ - u^-|) \, d\mathcal{H}^{d-1} \\ &= \sum_{(i,j) \in E} \int_{\Gamma_{ij}} \kappa(|c_i - c_j|) \, d\mathcal{H}^{d-1} \\ &= \sum_{(i,j) \in E} \kappa(|c_i - c_j|) \int_{\Gamma_{ij}} d\mathcal{H}^{d-1} \\ &= \sum_{(i,j) \in E} w_{ij} \kappa(|c_i - c_j|), \\ &=: R_\Pi(c) \end{aligned} \tag{8}$$

identifying the weights $w_{ij} = \int_{\Gamma_{ij}} d\mathcal{H}^{d-1} = |\Gamma_{ij}|$. With this weighting we can define the weighted finite graph $G = (V, E, w)$ as the discrete graph structure with which any continuous function $u \in BV_\Pi(\Omega, \mathbb{R}^L)$ can be represented. Note that if κ is the identity, then $R_\Pi(c)$ is equivalent to graph total variation of c (cf. [18, 6]).

Constraint Set:

We are further carrying a constraint set when minimizing the minimal partitions problem. However, both constraints are pointwise and therefore straight forward to relate to constraints on c_i , i.e., the constraint set

$$C = \left\{ u \mid u_k(x) \in [0, 1], \sum_{k=1}^L u_k(x) = 1 \right\}$$

directly translates to

$$C_\Pi = \left\{ c \mid (c_i)_k \in [0, 1], \sum_{k=1}^L (c_i)_k = 1, \forall i \right\}.$$

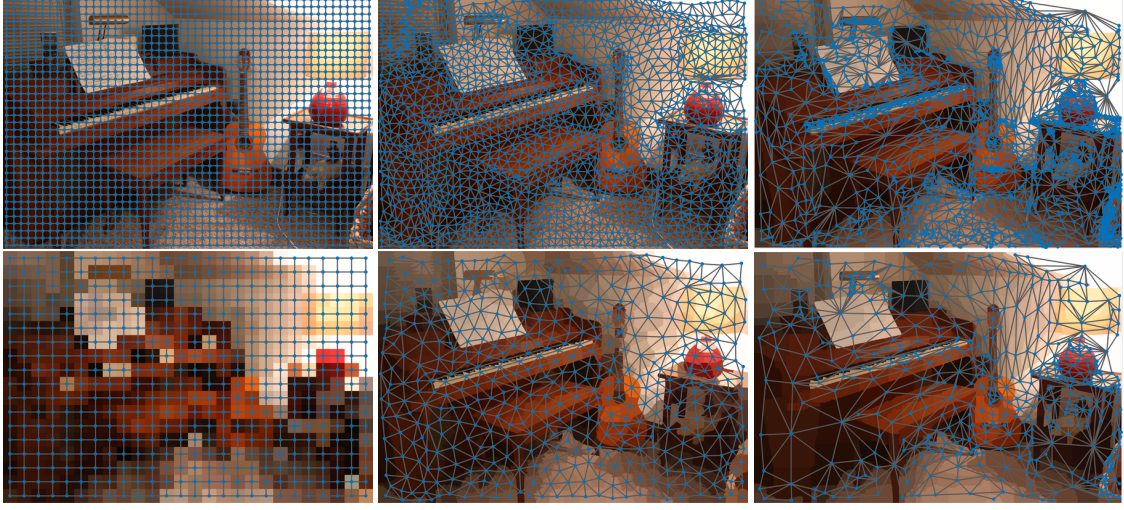


Figure 3: From left to right: Grid Sampling, SLIC Superpixels and L^0 Cut-Pursuit. Images from the Middlebury dataset[48]. The top row shows a fine discretization into the same number of nodes for every method, whereas the lower row shows a coarse discretization with the same number of nodes for every method.

Interestingly, the above restriction from the minimization of F over $BV(\Omega, \mathbb{R}^L)$ to its minimization over $BV_\Pi(\Omega, \mathbb{R}^L)$ (which translates into the minimization of F_Π over $c \in C_\Pi$) remains valid as long as the jump set of the true solution is a subset of the jumps in the partition Π , independent of what exactly the "super" jump-set of Π is. Let us formalize this result:

Proposition 1. *Assume a discretization Π and its assorted partitions P_i to be given. Let u^* be a minimizer to the continuous problem Eq. (2) for given potentials f_k . If the jump-set J_{u^*} of u^* is a subset of the jump set of Π given as the boundaries $\cup_{(i,j) \in E} \Gamma_{ij}$, then*

$$\min_{u \in C} F(u) = \min_{c \in C_\Pi} F_\Pi(c),$$

for the discrete energy $F_\Pi = K_\Pi + R_\Pi$, i.e. the continuous minimum $F(u^*)$ is equal to the minimum $F_\Pi(c^*)$ of the discrete energy of F_Π under the constraints C_Π .

Proof. See appendix. □

Proposition 1 directly implies that under the given assumptions one can construct the real optimum u^* of the continuous problem by computing the minimizer c^* of the function F_Π numerically on a finite graph. Practically however, we now need to find some partition Π that approximates (or ideally overestimates) the true jump set J_{u^*} , but consists of a limited number of segments.

Thus, the aim is to find a good approximation of given data preserving as many possible jumps in the candidate data as possible and catching the varying level of detail by different sized segments in Π to have high efficiency for minimization methods. On a Cartesian grid, the equivalent operation is to downsample the image, result in the "superpixels" seen in Fig. 3 on the left, which are not well aligned with edges in the images. However approaches such as SLIC (middle) or Cut-Pursuit (right, in the variant of [53]) are more adept at finding a superset of candidate partitions.



Figure 4: Illustrating the use of model-based segmentation methods: The user scribbles different objects to be segmented (left) from which a unary data term f is generated, e.g. by approaches like [37] or a pointwise neural network. As the unaries are insufficient for a good segmentation (illustrated by the fact that a thresholding of the unaries shown in the middle does not segment the background well), the proposed framework offers an efficient approach to obtain accurate segmentations as shown on the right.

4 Numerical Evaluation

This section focuses on evaluating the proposed approach. We discuss examples in segmentation and stereo estimation. For segmentation we show a practical example, where the approach is used to align the output of a pixelwise neural network. We then follow up with a detailed comparison of graphs generated by SLIC, Cut Pursuit and downsampling. In many computer vision applications, we are working with discrete image data, captured from high-resolution cameras or video devices. To apply our methodology, we need to consider that the finest possible discretization is given by the sensor grid. Incoming high resolution images are usually downsampling before applying costly computer vision procedures. This is of course a specific form of discretization to a smaller grid, and analogously we could apply a superpixel approach to generate the smaller discretization.

4.1 Segmentation

Multi-label segmentation is a central application of minimal partition problems, having been discussed in the continuous setting in works such as [12, 40] and widely studied in discrete methods such as [4, 26].

To apply multilabel segmentation we use the model described in Eq. (1), which can be recovered from Eq. (5) by setting $\kappa = \text{Id}$ and choosing the L^1 norm for $|\cdot|$, leading to an anisotropic penalty of the jumps.

Use Case:

As one application scenario, imagine a user wants to segment an image by marking the objects to be segmented with scribbles, see Fig. 4 on the left. Once the scribbling is complete we train a tiny pixelwise fully connected network on classifying the scribbled pixels correctly. For this experiment we used the colors and coordinates as features to be classified via a 2-hidden-layer fully network with batchnorm and ReLU activations with 6 and 12 hidden neurons. Due to the tiny architecture and the few scribbles, the training of the network takes 18 seconds on a Laptop CPU (without fine-tuning the hyperparameters), and inferring pixelwise unaries on the entire 1440×1920 pixel image takes less than a second. While solving the full segmentation problem with 15 labels requires 6 GB of memory, the proposed approach reduces the memory requirements to 0.2 GB due to the graph construction and needs only 13% of computation time in total to yield the segmentation shown in Fig. 4 on the right, which is precise enough to conduct various image manipulations such as inserting or removing some of the bottles or fruits.

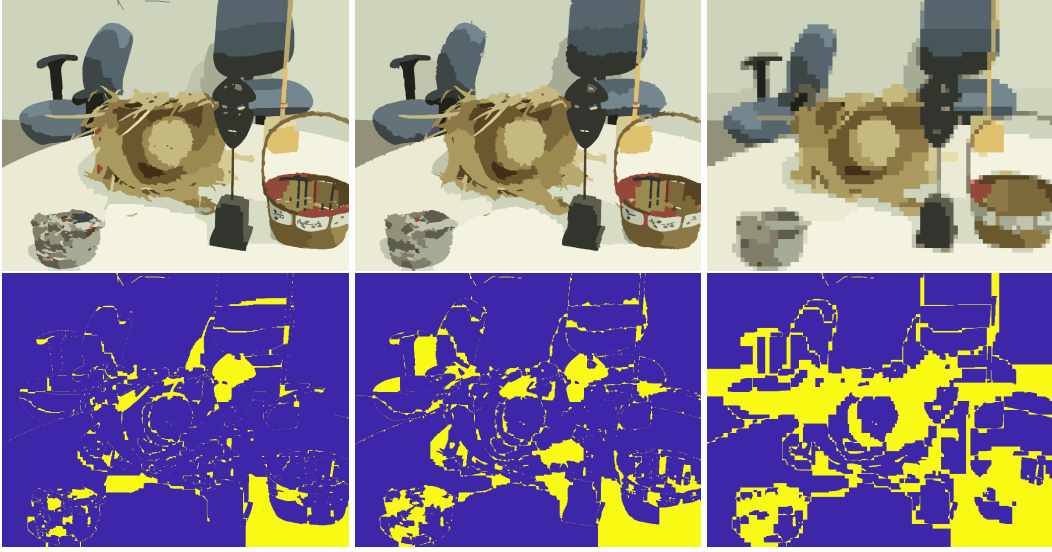


Figure 5: Qualitative comparison of image segmentation methods using the L^0 -CP graph (top), the SLIC graph (middle), and a rectangular grid (bottom). The graphs are constructed as described in Section 3.2. The left images show the final minimal partition result. The right images show the errors compared to the minimal partition computed on the full pixel grid.

Quantitative Analysis:

To analyze a wide range of images with canonical potentials, we turn to cartooning, i.e. multi-label segmentation with a fixed set of target colors chosen by a k-means selection. We hence have the following potentials for a given image $I : \Omega \rightarrow \mathbb{R}^3$:

$$f_k(x) = -\|I(x) - (c_k)\|_2^2, \quad (9)$$

for $\{c_k\}_{k=1}^L$ target colors for each label $1, \dots, L$. We directly choose $I = g$ for the Cut-Pursuit algorithm input. Figure 5 visualizes the result of the minimal partition problem for our graph discretization via L^0 -CP, a graph constructed via SLIC, and a subsampling of the pixel grid, all with the same number of vertices. We see that the partition problem can be solved well on these much smaller graph structure. Checking the error maps on the right-hand side of Fig. 5 we see that both superpixel methods lead to solutions that closely match the solution at the finest level, while the downsampling is comparatively error-prone. Note further that the L^0 -CP constructed discretization finally outperforms the SLIC-based discretization, due to its closer adherence to image edges.

This behavior can also be seen in Fig. 6 which shows a quantitative comparison, where several reduction rates, controlled by α_c for the Cut-Pursuit method and matched for the SLIC method and grid sampling. The methods are compared with regard to the amount of time saved and with regard to the number of nodes in the smaller graph discretization. Note that we always denote the measured time as the sum of the time used for the reduction method and the computational time to solve the label problem. Interestingly energy values can be matched very closely using the superpixel-based graph discretization, in stark contrast to the downsampling of the image grid.

In Table 1 we compare the three methods for three different example datasets. As we can see, solving on the smaller graph discretizations yields a huge improvement in runtime and uses a significantly less memory. Still the energies are close to the original energy one obtains by solving on the entire pixel grid. Considering the energy offsets in combination with the time saved we can deduce that the L^0 -CP is superior to the other

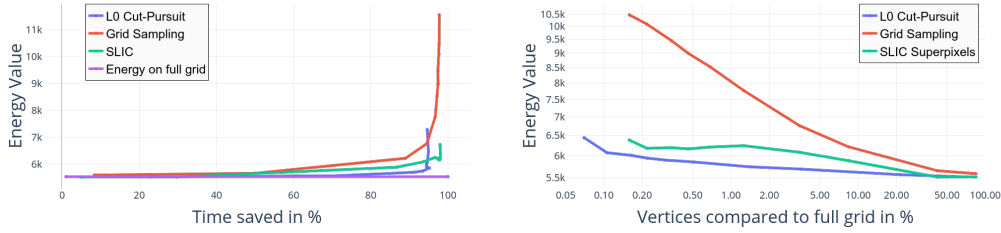


Figure 6: Computing the minimal partition on a well chosen graph discretization is much more efficient than computing it on the full grid. Left: Time saved vs 100% on the full grid plotted vs the partition energy of the minimizer. Right: The number of nodes compared to the partition energy of the minimizer.

Ex.	Methods	Red. Rate	Time Saved	Mem.	Energy Offset
1	L^0 -CP	31%	79%	15MB	0.73%
	SLIC	41%	41%	16MB	1.18%
	sampling	74%	22%	32MB	5.77%
2	L^0 -CP	3.6%	87%	12MB	3.5%
	SLIC	8.42%	87%	32MB	6.29%
	sampling	8.42%	87%	27MB	13.33%
3	L^0 -CP	6.2%	83%	463MB	2.1%
	SLIC	14%	79%	1144MB	4.43%
	sampling	14%	82%	2976MB	3.79%

Table 1: Different scores for three examples: 1. "cedar.bmp"[57], 2. "fish.jpg"[33], 3. "bin.png"[48], computed for a multi-label segmentation with $L = 16$ labels. *Reduction Rate* is the ratio between the number of segments to the full number of nodes. *Time save* describes the ratio of time that was saved by the graph discretization and *Energy offset* the ratio of energy mismatch. The baseline method uses 301, 684 and 6113 MB for every experiment respectively.

methods. Combining these figures we observe that graph-based discretization leads to a significant improvement in accuracy, compared to computing the segmentation on a downsampled grid, and further that using the L^0 -CP superpixels leads to the most efficient final result, even though the computation of these superpixels itself takes more time than SLIC (the time to compute superpixels and construct the graph is factored into all measurements we consider).

4.2 Implementation Details

We implement the graph-structured optimization of the convexified partition problem via a primal-dual algorithm [10] with diagonal preconditioning [39]. The preconditioning allows us to reconcile the step sizes of the algorithm with the varying sizes of the graph partitions. We use the implementation of this algorithm from <https://github.com/tum-vision/prost>, which conducts GPU computations with a Matlab wrapper. The L^0 -CP implementation is written in Matlab using just the internal *maxflow* implementation.

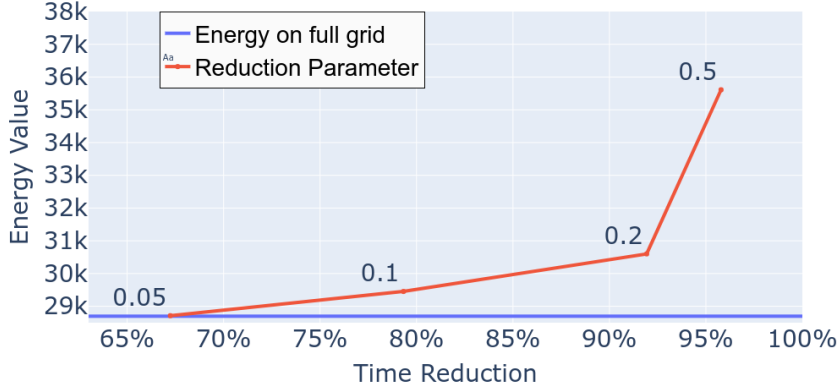


Figure 7: Illustration of the trade-off between the time reduction achieved by the Cut-Pursuit and the energy values. Depicted are the different adjustments of α_c .

4.3 Stereo Matching

For the task of estimating disparities in stereo images the problem setting is different from that of segmentation tasks. While we want to reconstruct discrete labels for segmentation the estimated disparities between images live in a continuous range and therefore need dedicated treatment. The one-hot vector structure of discrete segmentation labels ideally has to be translated to a continuously metricized label space. Though it is possible to tackle stereo matching with a label-based lifting approach like [42], more involved techniques have emerged reducing the amount of labels whilst admitting a richer class of cost functions [35].

Assuming piecewise constant disparities in natural images it is still possible to transfer the graph reduction ideas to the sublabel accurate setting of [36]. Attention has to be paid to the treatment of the data term, however, as it does not bear the linear structure with respect to the label coefficients anymore.

Quantitative Analysis:

As the data term for stereo matching can be expressed as a cost-vector defined for each pixel, we need to find a sensitive scalar data function where superpixels can be computed to construct the graph. A natural choice for such a function is the pixelwise minimizing argument of the data term. This is motivated by the intuition that constant regions of pointwise minimizing disparities likely induce constant regions of the original data term. As for segmentation we have a large variety of unaries we can choose for calculating the data term for disparities. Even though one could pick more sophisticated unaries, like outputs of certain neural networks, we stick with the comparison of the truncated image gradients to showcase the benefits of our method in a more confined setting.

Remark. As mentioned earlier the non-linearity of the data term w.r.t. the label coefficients impedes the direct application of the proposed graph reduction. A closer look on the stereo problem formulation of [36] reveals that the data term in between two neighboring labels is formed by calculating the convex envelope over the finitely sampled disparity costs. To be more precise, the stereo matching cost can be regarded as a in general non-linear data term $f_x: \mathbb{R}^L \rightarrow \mathbb{R}$ for each $x \in \Omega$. It directly operates on the lifted variable function $u: \Omega \rightarrow \mathbb{R}^L$. The data term is then relaxed to f_x^{**} for each x . This eventually amounts to a piecewise linear data term for each interval. Summing the data terms over superpixels, however, even yields a tighter convex approximation as

$$\sum_{i=1}^M \left(\int_{P_i} f_x dx \right)^{**} \geq \int_{\Omega} f_x^{**} dx, \quad (10)$$

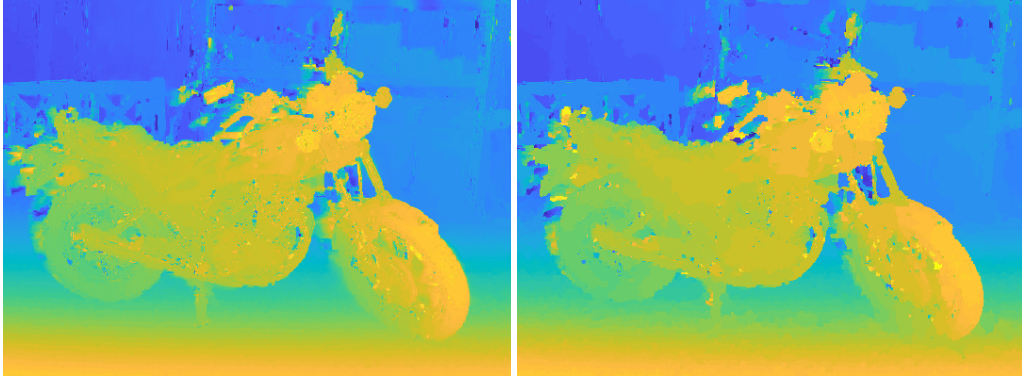


Figure 8: A stereo matching result computed on the full image (left) is compared to the result on the reduced problem computed using the proposed approach. Both methods use a sublabel approach [36] on 32 labels. The Cut-Pursuit parameter was picked as $\alpha_c = 0.1$ amounting to a time reduction by a factor of 4.8.

where the left data term is the one effectively used when applying the method from [36] to superpixels as discussed.

Figure 7 shows the time reduction vs. the achieved energy values of our method compared to the full stereo matching problem. Note the scale of the x-axis. We can easily reduce the necessary time and memory costs by using the graph-based discretization. Figure 8 gives a visual impression of the approximation behavior of the graph reduction on an exemplary stereo image. Despite of the significant speedup for stereo matching the proposed method still is capable of producing visually pleasing results, as the matching is still computed with respect to all variables, just with an optimally chosen discretization.

5 Conclusions

In this work we presented strategies for the efficient computation of convex relaxations by directly moving from geometric properties of minimal partitions solutions to a graph-based discretization. We find that such a graph-based discretization can be constructed in adherence to the global partitioning problem. Constructing this graph for superpixels given by SLIC or Cut-Pursuit approaches yields accurate and efficient solutions in practice, leading an improved spatial discretization of the matching problem - compared to a Cartesian grid. We further find that using a superpixel approach that is more faithful to minimal surface energies, as the L^0 -Cut Pursuit algorithm leads to more accurate solutions compared to SLIC and can be well worth the additional effort. We believe that the proposed methodology can facilitate the use of convex relaxation methods in practical applications, especially if input data is of high-resolution, where memory and computation constraints made these approaches previously infeasible.

References

- [1] Radhakrishna Achanta, Appu Shaji Shaji, Kevin Smith, Aurelien Lucchi, Pascal Fua, and Sabine Süsstrunk. SLIC Superpixels Compared to State-of-the-Art Superpixel Methods. *IEEE Trans. Pattern Anal. Mach. Intell.*, 34(11):2274–2282, November 2012. 3, 17
- [2] Luigi Ambrosio, Nicola Fusco, and Diego Pallara. *Functions of Bounded Variation and Free Discontinuity Problems*. Oxford university press, Oxford, 2000. 4

- [3] Yuri Boykov and Gareth Funka-Lea. Graph Cuts and Efficient N-D Image Segmentation. *Int. J. Comput. Vis.*, 70(2):109–131, November 2006. [1](#), [2](#), [3](#), [18](#)
- [4] Yuri Boykov, Olga Veksler, and Ramin Zabih. Fast approximate energy minimization via graph cuts. *IEEE Trans. Pattern Anal. Mach. Intell.*, 23(11):1222–1239, November 2001. [2](#), [3](#), [8](#), [17](#)
- [5] Kristian Bredies, Thomas Pock, and Benedikt Wirth. A Convex, Lower Semicontinuous Approximation of Euler’s Elastica Energy. *SIAM J. Math. Anal.*, 47(1):566–613, January 2015. [3](#)
- [6] Xavier Bresson and Tony F. Chan. Non-local Unsupervised Variational Image Segmentation Models. UCLA CAM report, University of California, Los Angeles, 2008. [6](#)
- [7] Thomas Brox, Andrés Bruhn, Nils Papenberg, and Joachim Weickert. High Accuracy Optical Flow Estimation Based on a Theory for Warping. In *Computer Vision - ECCV 2004*, volume 3024, pages 25–36. Springer Berlin Heidelberg, Berlin, Heidelberg, 2004. [1](#)
- [8] Martin Burger and Stanley Osher. A Guide to the TV zoo. In *PDE Based Reconstruction Methods in Imaging*, number 2090 in Lecture Notes in Mathematics. Springer International Publishing, Switzerland, 1 edition, 2013. [3](#), [17](#)
- [9] Antonin Chambolle, Daniel Cremers, and Thomas Pock. A Convex Approach to Minimal Partitions. *SIAM J. Imaging Sci.*, 5(4):1113–1158, October 2012. [2](#), [3](#), [4](#), [5](#)
- [10] Antonin Chambolle and Thomas Pock. A First-Order Primal-Dual Algorithm for Convex Problems with Applications to Imaging. *J Math Imaging Vis*, 40(1):120–145, May 2011. [10](#), [17](#)
- [11] Tony F. Chan, Selim Esedoglu, and Mila Nikolova. Algorithms for Finding Global Minimizers of Image Segmentation and Denoising Models. *SIAM J. Appl. Math.*, 66(5):1632–1648, January 2006. [2](#)
- [12] Tony F. Chan and Luminita A. Vese. Active contours without edges. *IEEE Trans. Image Process.*, 10(2):266–277, 2001. [8](#)
- [13] Liang-Chieh Chen, George Papandreou, Iasonas Kokkinos, Kevin Murphy, and Alan L. Yuille. DeepLab: Semantic Image Segmentation with Deep Convolutional Nets, Atrous Convolution, and Fully Connected CRFs. *ArXiv160600915 Cs*, June 2016. [2](#)
- [14] Daniel Cremers, Thomas Pock, Kalin Kolev, and A. Chambolle. Convex Relaxation Techniques for Segmentation, Stereo and Multiview Reconstruction. In *Markov Random Fields for Vision and Image Processing*. MIT Press, Boston, 2011. [2](#), [3](#)
- [15] Jonathan Eckstein and Dimitri P. Bertsekas. On the Douglas—Rachford splitting method and the proximal point algorithm for maximal monotone operators. *Mathematical Programming*, 55(1):293–318, April 1992. [17](#)
- [16] Abderrahim Elmoataz, Olivier Lezoray, and Sébastien Bougleux. Nonlocal Discrete Regularization on Weighted Graphs: A framework for Image and Manifold Processing. *IEEE Trans. Image Process.*, 17(7):1047–1060, 2008. [3](#)
- [17] Herbert Federer. *Geometric Measure Theory*. Classics in Mathematics. Springer-Verlag, Berlin Heidelberg, 1996. [4](#)
- [18] Guy Gilboa and Stanley Osher. Nonlocal Operators with Applications to Image Processing. *Multiscale Model. Simul.*, 7(3):1005–1028, November 2008. [6](#)
- [19] Bastian Goldluecke, Evgeny Strelakovsky, and Daniel Cremers. Tight Convex Relaxations for Vector-Valued Labeling. *SIAM J. Imaging Sci.*, 6(3):1626–1664, January 2013. [3](#)
- [20] Stéphane Guinand, Loïc Landrieu, Laurent Caraffa, and Bruno Vallet. Piecewise-Planar Approximation of Large 3D Data as Graph-Structured Optimization. In *ISPRS Annals of Photogrammetry, Remote Sensing and Spatial Information Sciences*, volume IV-2-W5, pages 365–372. Copernicus GmbH, May 2019. [3](#)
- [21] Berthold K. P. Horn and Brian G. Schunck. Determining optical flow. *Artificial Intelligence*, 17(1):185–203, August 1981. [1](#), [2](#)
- [22] Hiroshi Ishikawa. Exact optimization for Markov random fields with convex priors. *IEEE Trans. Pattern Anal. Mach. Intell.*, 25(10):1333–1336, October 2003. [3](#)
- [23] Hiroshi Ishikawa and Davi Geiger. Occlusions, discontinuities, and epipolar lines in stereo. In *Computer Vision — ECCV’98*, Lecture Notes in Computer Science, pages 232–248. Springer Berlin Heidelberg, 1998. [1](#), [3](#)
- [24] Hiroshi Ishikawa and Davi Geiger. Segmentation by Grouping Junctions. In *Proceedings of the IEEE Computer Society Conference on Computer Vision and Pattern Recognition*, CVPR ’98, pages 125–, Washington, DC, USA, 1998. IEEE Computer Society. [3](#)
- [25] Kalin Kolev and Daniel Cremers. Integration of Multiview Stereo and Silhouettes Via Convex Functionals on Convex Domains. In *Computer Vision – ECCV 2008*, Lecture Notes in Computer Science, pages 752–765, Berlin, Heidelberg, 2008. Springer. [2](#), [3](#)
- [26] Vladimir Kolmogorov and Ramin Zabih. What energy functions can be minimized via graph cuts? *IEEE Trans. Pattern Anal. Mach. Intell.*, 26(2):147–159, February 2004. [3](#), [8](#)
- [27] Loïc Landrieu and Guillaume Obozinski. Cut Pursuit: Fast algorithms to learn piecewise constant functions. In *Proceedings of the 19th International Conference on Artificial Intelligence and Statistics*, volume 51 of *Proceedings of Machine Learning Research*, pages 1384–1393, Cadiz, Spain, April 2016. PMLR. [3](#), [17](#), [18](#)

- [28] Loic Landrieu and Guillaume Obozinski. Cut Pursuit: Fast Algorithms to Learn Piecewise Constant Functions on General Weighted Graphs. *SIAM J. Imaging Sci.*, 10(4):1724–1766, January 2017. 3
- [29] Loic Landrieu and Martin Simonovsky. Large-scale Point Cloud Semantic Segmentation with Superpoint Graphs. *ArXiv171109869 Cs*, November 2017. 3
- [30] Emanuel Laude, Thomas Möllenhoff, Michael Moeller, Jan Lellmann, and Daniel Cremers. Sublabel-Accurate Convex Relaxation of Vectorial Multilabel Energies. In *Computer Vision – ECCV 2016*, Lecture Notes in Computer Science, pages 614–627. Springer, Cham, October 2016. 3
- [31] Jan Lellmann, Jörg Kappes, Jing Yuan, Florian Becker, and Christoph Schnörr. Convex Multi-class Image Labeling by Simplex-Constrained Total Variation. In *Scale Space and Variational Methods in Computer Vision*, Lecture Notes in Computer Science, pages 150–162. Springer Berlin Heidelberg, 2009. 2, 3
- [32] Jan Lellmann, Evgeny Strekalovskiy, Sabrina Koetter, and Daniel Cremers. Total Variation Regularization for Functions with Values in a Manifold. In *Proceedings of the 2013 IEEE International Conference on Computer Vision, ICCV '13*, pages 2944–2951, Washington, DC, USA, 2013. IEEE Computer Society. 3
- [33] David Martin, Charles Fowlkes, Doron Tal, and Jitendra Malik. A Database of Human Segmented Natural Images and its Application to Evaluating Segmentation Algorithms and Measuring Ecological Statistics. In *Proceedings of 8th International Conference on Computer Vision*, volume 2, pages 416–423, July 2001. 10
- [34] David Mumford and Jayant Shah. Optimal approximations by piecewise smooth functions and associated variational problems. *Commun. Pure Appl. Math.*, 42(5):577–685, 1989. 1, 3
- [35] Thomas Möllenhoff and Daniel Cremers. Sublabel-Accurate Discretization of Nonconvex Free-Discontinuity Problems. *Proc. IEEE Int. Conf. Comput. Vis.*, pages 1183–1191, August 2017. 3, 4, 5, 11
- [36] Thomas Möllenhoff, Emanuel Laude, Michael Moeller, Jan Lellmann, and Daniel Cremers. Sublabel-Accurate Relaxation of Nonconvex Energies. In *Proceedings of the IEEE Conference on Computer Vision and Pattern Recognition*, pages 3948–3956, 2016. 3, 11, 12
- [37] Claudia Nieuwenhuis, Eno Töppe, and Daniel Cremers. A Survey and Comparison of Discrete and Continuous Multi-label Optimization Approaches for the Potts Model. *Int J Comput Vis*, 104(3):223–240, September 2013. 3, 8
- [38] T. Pock, C. Zach, and H. Bischof. Mumford-Shah Meets Stereo: Integration of Weak Depth Hypotheses. In *2007 IEEE Conference on Computer Vision and Pattern Recognition*, pages 1–8, June 2007. 2
- [39] Thomas Pock and Antonin Chambolle. Diagonal preconditioning for first order primal-dual algorithms in convex optimization. In *2011 International Conference on Computer Vision*, pages 1762–1769, November 2011. 10, 18
- [40] Thomas Pock, Antonin Chambolle, Daniel Cremers, and Horst Bischof. A convex relaxation approach for computing minimal partitions. In *Computer Vision and Pattern Recognition, 2009. CVPR 2009. IEEE Conference On*, pages 810–817. IEEE, 2009. 3, 8
- [41] Thomas Pock, Daniel Cremers, Horst Bischof, and Antonin Chambolle. An algorithm for minimizing the Mumford-Shah functional. In *2009 IEEE 12th International Conference on Computer Vision*, pages 1133–1140. IEEE, 2009. 3
- [42] Thomas Pock, Daniel Cremers, Horst Bischof, and Antonin Chambolle. Global Solutions of Variational Models with Convex Regularization. *SIAM J. Imaging Sci.*, 3(4):1122–1145, January 2010. 2, 3, 11
- [43] Thomas Pock, Thomas Schoenemann, Gottfried Graber, Horst Bischof, and Daniel Cremers. A convex formulation of continuous multi-label problems. In *European Conference on Computer Vision*, pages 792–805. Springer, 2008. 2, 3
- [44] Renfrey Burnard Potts. Some generalized order-disorder transformations. In *Mathematical Proceedings of the Cambridge Philosophical Society*, volume 48, pages 106–109. Cambridge Univ Press, 1952. 2
- [45] Rene Ranftl, Stefan Gehrig, Thomas Pock, and Horst Bischof. Pushing the limits of stereo using variational stereo estimation. In *Intelligent Vehicles Symposium (IV), 2012 IEEE*, pages 401–407. IEEE, 2012. 1, 3
- [46] Rene Ranftl, Thomas Pock, and Horst Bischof. Minimizing TGV-Based Variational Models with Non-convex Data Terms. In *Scale Space and Variational Methods in Computer Vision*, Lecture Notes in Computer Science, pages 282–293. Springer Berlin Heidelberg, June 2013. 3
- [47] Leonid I. Rudin, Stanley Osher, and Emad Fatemi. Nonlinear total variation based noise removal algorithms. *Physica D: Nonlinear Phenomena*, 60(1):259–268, November 1992. 3, 17
- [48] Daniel Scharstein, Heiko Hirschmüller, York Kitajima, Greg Krathwohl, Nera Nešić, Xi Wang, and Porter Westling. High-Resolution Stereo Datasets with Subpixel-Accurate Ground Truth. In *Pattern Recognition*, Lecture Notes in Computer Science, pages 31–42. Springer, Cham, September 2014. 7, 10
- [49] Mohamed Souiai, Martin R. Oswald, Youngwook Kee, Junmo Kim, Marc Pollefeys, and Daniel Cremers. Entropy Minimization for Convex Relaxation Approaches. In *Proceedings of the IEEE International Conference on Computer Vision*, pages 1778–1786, 2015. 3

- [50] Evgeny Strekalovskiy, Antonin Chambolle, and Daniel Cremers. Convex Relaxation of Vectorial Problems with Coupled Regularization. *SIAM J. Imaging Sci.*, 7(1):294–336, January 2014. [2](#), [3](#)
- [51] Evgeny Strekalovskiy and Daniel Cremers. Real-Time Minimization of the Piecewise Smooth Mumford-Shah Functional. In *Computer Vision – ECCV 2014*, Lecture Notes in Computer Science, pages 127–141. Springer, Cham, September 2014. [17](#)
- [52] Evgeny Strekalovskiy, Bastian Goldluecke, and Daniel Cremers. Tight convex relaxations for vector-valued labeling problems. In *2011 International Conference on Computer Vision*, pages 2328–2335, November 2011. [2](#), [3](#)
- [53] Daniel Tenbrinck, Fjedor Gaede, and Martin Burger. Variational Graph Methods for Efficient Point Cloud Sparsification. *ArXiv190302858 Cs Math*, March 2019. [7](#), [17](#), [18](#)
- [54] Roy Uziel, Meitar Ronen, and Oren Freifeld. Bayesian Adaptive Superpixel Segmentation. In *Proceedings of the IEEE International Conference on Computer Vision*, pages 8470–8479, 2019. [3](#)
- [55] Manuel Werlberger, Markus Unger, Thomas Pock, and Horst Bischof. Efficient Minimization of the Non-local Potts Model. In *Scale Space and Variational Methods in Computer Vision*, Lecture Notes in Computer Science, pages 314–325. Springer Berlin Heidelberg, May 2011. [3](#)
- [56] Thomas Windheuser and Daniel Cremers. A Convex Solution to Spatially-Regularized Correspondence Problems. In *Computer Vision – ECCV 2016*, Lecture Notes in Computer Science, pages 853–868, Cham, 2016. Springer International Publishing. [3](#)
- [57] John M Winn, Antonio Criminisi, and Thomas P Minka. Object categorization by learned universal visual dictionary. In *Tenth IEEE International Conference on Computer Vision (ICCV’05) Volume 1*, volume 2, pages 1800–1807 Vol. 2, October 2005. [10](#)
- [58] Christopher Zach. Robust bundle adjustment revisited. In *European Conference on Computer Vision*, pages 772–787. Springer, 2014. [3](#)
- [59] Christopher Zach, David Gallup, Jan-Michael Frahm, and Marc Niethammer. Fast Global Labeling for Real-Time Stereo Using Multiple Plane Sweeps. In *Vision, Modeling, and Visualization*, pages pp. 243–252, Amsterdam, The Netherlands, August 2008. IOS Press. [2](#)
- [60] Christopher Zach, Christian Häne, and Marc Pollefeys. What is optimized in tight convex relaxations for multi-label problems? In *2012 IEEE Conference on Computer Vision and Pattern Recognition*, pages 1664–1671, June 2012. [3](#)
- [61] Christopher Zach, Thomas Pock, and Horst Bischof. A Duality Based Approach for Realtime TV-L1 Optical Flow. In *Pattern Recognition*, pages 214–223. Springer, Berlin, Heidelberg, September 2007. [2](#), [3](#)

A Proof of Proposition 1

We intend to show [Proposition 1](#) by first showing a lemma for functionals of the form

$$\begin{aligned}
 F(u) = & \int_{\Omega \setminus J_u} \Phi(x, u(x), \nabla u(x)) \, dx \\
 & + \int_{J_u} \kappa(|u^+ - u^-|) |\nu_u| d\mathcal{H}^{d-1},
 \end{aligned} \tag{5}$$

for $u \in SBV(\Omega, \mathbb{R}^L)$ under constraints C given as

$$C = \left\{ u \mid u_k(x) \in [0, 1], \sum_{k=1}^L u_k(x) = 1 \right\}.$$

Lemma A.1. Assume a discretization Π and its assorted partitions P_i to be given. Let u^* be a minimizer to the continuous problem [Eq. \(5\)](#). If the jump-set J_{u^*} of u^* is a subset of the jump set of Π given as the boundaries $\cup_{(i,j) \in E} \Gamma_{ij}$, then

$$\min_{u \in C} F(u) = \min_{c \in C_\Pi} F_\Pi(c),$$

for the discrete energy $F_\Pi = K_\Pi + R_\Pi$, i.e. the continuous minimum $F(u^*)$ is equal to the minimum $F_\Pi(c^*)$ of the discrete energy of F_Π under the constraints C_Π .

Proof. As defined in Section 3.2 of the main paper, we consider the space $BV_{\Pi}(\Omega, \mathbb{R}^L)$ of functions in $BV(\Omega, \mathbb{R}^L)$ that are piecewise-constant on partition Π . From the assumption that J_{u^*} is a subset of the jump set of Π , given by $\bigcup_{(i,j) \in E} \Gamma_{ij}$, we deduce $u^* \in BV_{\Pi}(\Omega, \mathbb{R}^L)$. For a partition Π define

$$\Xi_{\Pi} = \{u \in C \mid u \in BV_{\Pi}(\Omega, \mathbb{R}^L)\},$$

for

$$C = \{u \mid u_k(x) \in [0, 1], \sum_{k=1}^L u_k(x) = 1\}.$$

Then $\Pi' \leq \Pi$, where " \leq " refers to the partial order on partitions meaning Π' is a finer partition than Π . This implies $\Xi_{\Pi} \subseteq \Xi_{\Pi'}$. For $u \in C_{\Pi}$ and the according c from Section 3.2 we already have shown $F_{\Pi}(c) = F(u)$.

Hence, $u^* \in \Xi_{\Pi}$ allows us to write

$$\begin{aligned} \min_{c \in C_{\Pi}} F_{\Pi}(c) &= \min_{\tilde{u} \in \Xi_{\Pi}} F(\tilde{u}) \\ &\leq F(u^*) = \min_{u \in C} F(u). \end{aligned}$$

Equality now follows due to $\Xi_{\Pi} \subseteq C$ from

$$\min_{u \in C} F(u) \leq \min_{\tilde{u} \in \Xi_{\Pi}} F(\tilde{u}) = \min_{c \in C_{\Pi}} F_{\Pi}(c).$$

□

Now we can find proposition 1 as a simply corollary. The minimal partitions problem

$$\min_{\{u_k\}_{k=1}^L} \sum_{k=1}^L \int_{\Omega} -f_k(x)u_k(x) + \int_{\Omega} |Du_k|, \quad (1)$$

is a special case of Eq. (5) by choosing the data term via

$$K_{\Pi}(c) = \sum_{k=1}^L \sum_{i=1}^M (c_i)_k \int_{P_i} f_k(x) dx = \sum_{i=1}^M \langle c_i, \tilde{f}_k \rangle. \quad (7)$$

and setting $\kappa = Id$ for the regularization term.

Proposition 1. Assume a discretization Π and its assorted partitions P_i to be given. Let u^* be a minimizer to the continuous problem Eq. (2) for given potentials f_k . If the jump-set J_{u^*} of u^* is a subset of the jump set of Π given as the boundaries $\bigcup_{(i,j) \in E} \Gamma_{ij}$, then

$$\min_{u \in C} F(u) = \min_{c \in C_{\Pi}} F_{\Pi}(c),$$

for the discrete energy $F_{\Pi} = K_{\Pi} + R_{\Pi}$, i.e. the continuous minimum $F(u^*)$ is equal to the minimum $F_{\Pi}(c^*)$ of the discrete energy of F_{Π} under the constraints C_{Π} .

Proof. Apply Lemma A.1 to Eq. (2). □

B Algorithmic Details

For implementation reference we replicate some parts of the L^0 Cut-Pursuit [27] variant of [53] in the continuous setting.

To obtain a good trade-off between having as few segments as possible but still constructing a partition whose jump set is a super set of the jump set of a minimizer u^* , we exploit a modification of the Cut-Pursuit (CP) algorithm of [27] discussed in [53]. In [27] Landrieu and Obozinski develop an approach to solve total variation problems [47, 8] with an alternating method solving graph cuts and reduced problems on the smaller graphs generated by these cuts. This is an efficient method with superior performance compared to more classical optimization methods as primal-dual [10] or Douglas-Rachford [15] algorithms minimizing the total variation problem. The Cut-Pursuit algorithm can be further extended to a variant minimizing the L^0 norm of the graph gradient. This strategy is able to quickly return approximate solutions to partitioning problems for a relatively high number of partitions compared to the number of potentials L we consider. The final number of partitions depends on regularization parameters and is data-dependent. In [53] Tenbrinck et. al. modify the Cut-Pursuit for L^0 by simplifying the algorithm to alternating between a graph cut and solving the data term separately on each generated partitions. We will denote this method as L^0 -Cut-Pursuit (L^0 -CP). We discuss this algorithm in a continuous setting with an L^2 data fidelity term, resulting in the following alternating algorithm: For a given function $u^k \in BV(\Omega, \mathbb{R})$ and some given data $g \in L^1(\Omega, \mathbb{R})$, one step of the algorithm consists of the two alternating optimization steps. The first one is

$$B^{k+1} = \operatorname{argmin}_{B \subset \Omega} \int_{\Omega} (u^k(x) - g(x)) 1_B(x) dx + \alpha_c \int_{\Omega} |D 1_B|, \quad (11)$$

where 1_B denotes a characteristic function on B . This set minimization in Eq. (11) is binary and thus globally solvable. Then compute Π^{k+1} as the connected components of B^{k+1} and, in a second step, find the mean over every partition,

$$c_i^{k+1} = \frac{1}{|P_i|} \int_{P_i} g(x) dx. \quad (12)$$

From the values c_i^{k+1} of the partitions $P_i \in \Pi^{k+1}$, we can compute the continuous solution via

$$u^{k+1} = \sum_{P_i \in \Pi^{k+1}} c_i^{k+1} 1_{P_i}. \quad (13)$$

Note that such an algorithm operates on $BV(\Omega, \mathbb{R})$ rather than $BV(\Omega, \mathbb{R}^L)$ in order to be much more efficient, particularly for large L .

Figure 3 illustrates the partitions P_i found by the above L^0 -CP (right) in comparison to a naive subsampling on a grid (left) and the SLIC superpixels from [1] for two different levels of discretizations. As we can see, the L^0 -CP generates less uniformly-sized regions, allowing to combine large constant regions into a single node in a graph and thus being well suited for an efficient coarsification with accurate edges. Algorithm 1 shows the steps that this algorithm follows for further clarification.

B.1 Implementation

On a discrete image grid generated by sensor data, Eq. (11) becomes a binary partitioning on a discrete graph, which can be solved efficiently by a *maxflow* algorithm, e.g. Boykov-Kolmogorov [4]. In the end variants, such as L^1 -Cut-Pursuit [27] or using a real-time Mumford-Shah such as [51] would also be possible candidates to find a candidate partition, yet we did not find these variants to yield either sufficient speed or sufficient accuracy around edges to be applicable - for algorithms that do not explicitly track the partitioning, the partition also has to be computed from the final result in an additional post-processing step.

Algorithm 1: L0-Pursuit from [53]

Result: Discretization Π

```
 $c^0 \leftarrow \text{mean}(g);$   
 $\Pi^0 \leftarrow \{\Omega\};$   
while  $\Pi^k \neq \Pi^{k+1}$  do  
   $B^{k+1} \leftarrow \text{Solve Eq. (11) for given } u^k;$   
   $\Pi^{k+1} \leftarrow \text{connected components of } B^{k+1};$   
   $c^{k+1} \leftarrow \text{Solve Eq. (12) for given } \Pi^{k+1};$   
   $u^{k+1} \leftarrow \text{Compute as in Eq. (13);}$   
   $k \leftarrow k + 1;$   
end  
 $\Pi \leftarrow \Pi^{k+1}$ 
```



Figure 9: Reduction of the raw image (left) to 6031 nodes in the graph structure (Right). In the middle we reproject the graph structure onto the original image, visualizing the high fidelity of the representation, even as the number of nodes reduces to 0.45% of the full grid.

When applying the Cut-Pursuit algorithm, we first need to consider which data will be used for g , the input to the Cut-Pursuit algorithm. A straightforward approach is to set

$$g(x) = \underset{k}{\operatorname{argmin}} f_k(x) \quad (14)$$

for the given label potentials, but especially for segmentation, using the color or grayscale image data directly is also reasonable under the assumption that piecewise constant objects in the RGB image correspond belong to separate labels, as done for algorithms such as SLIC.

We have chosen the `search-trees` implementation of [3] to solve the discrete version of the binary partition problem stated in Eq. (11). This can be done by reformulating the energy into a flow-graph structure with two additional terminal nodes *sink* and *source*. How to assign the right capacities to the edges can be taken from [27] or [53]. A significant bottleneck of this straightforward *maxflow* implementation is that the computation is difficult to parallelize. Thus, the computational time can increase drastically for very large images or other input data. For real-time applications with access to parallelization via GPUs or CPUs with sufficient cores we would recommend porting the entire pipeline into a single framework and using a primal dual algorithm with diagonal preconditioned stepsizes as in [39] not only for the minimal partitions problem but also the binary cuts. Especially running both subroutines on the GPU is potentially highly beneficial for large images. On the other hand, solving the binary cut with a primal-dual algorithm only approximates the solution in finite time and convergence criteria have to be chosen carefully to guarantee accurate results. In contrast *maxflow* termination criteria are straightforward, which is why we focus on *maxflow* in this work, aside from its applicability to weaker hardware with low specifications.

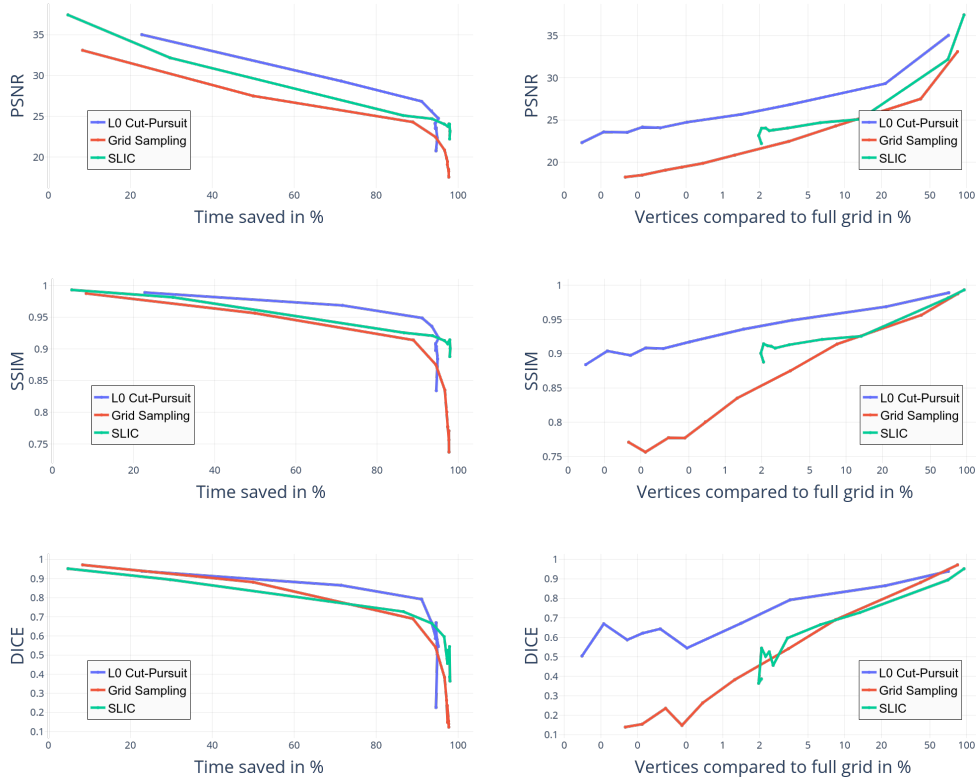


Figure 10: Computing the minimal partition on the graph is much more efficient than grid subsampling or SLIC superpixels. Left: Time saved vs 100% on the full grid plotted vs PSNR/SSIM/DICE score of the segmentation vs the full grid segmentation. Right: The number of nodes compared also compared to the PSNR/SSIM/DICE score of the segmentation.

C Further plots

Figure 9 shows the fidelity of the L0-Cut Pursuit representation of an RGB image. The reduction 0.45% in comparison to the full grid is hardly noticeable without zooming in. Figure 10 shows a variant of Figure 6 in the paper. We visualize PSNR / SSIM / DICE values for the cartooning problem. These are computed by reassembling the output image from the piecewise constant segmentation and comparing it to the input image.